Darlington pair of quantum thermal transistors

Ravi T. Wijesekara,[1,*] Sarath D. Gunapala,[2] and Malin Premaratne[1,†]
[1]*Advanced Computing and Simulation Laboratory(AχL), Department of Electrical and Computer Systems Engineering, Monash University, Clayton, Victoria 3800, Australia*
[2]*Jet Propulsion Laboratory, California Institute of Technology, Pasadena, California 91109, USA*

(Received 5 April 2021; revised 10 June 2021; accepted 21 June 2021; published 6 July 2021)

Recent progress in manipulating individual quantum systems has led to the development of quantum thermal transistors, which control the thermal conductivity between two of its terminals according to an input signal on its third terminal. With several models for individual thermal transistors already developed, the next natural step is to investigate how multiple thermal transistors can interconnect to build useful composite devices. In electronics literature, the Darlington pair is a two-transistor configuration commonly used to construct electronic amplifiers with higher gain than is possible with a single transistor. We create the electronic Darlington pair's thermal equivalent using two individual thermal transistors in a similar configuration. Unlike previously studied models, multitransistor configurations like this contain internal transistor interconnections whose temperatures cannot be biased externally but are determined by the individual transistors' internal dynamics. We refine previous models to incorporate these transistor-transistor interactions and introduce an intermediate thermal bath to facilitate the thermal energy exchange between the Darlington pair transistors. We investigate temperature-based and optical field-based control strategies of the Darlington pair in terms of both steady-state and transient thermal flow characteristics through numerical simulations. Under both control strategies, the thermal Darlington pair's steady-state performance exhibits superior thermal amplification, sensitivity, and thermodynamic efficiency than an equivalent single thermal transistor. Our results closely mirror those expected from the corresponding electronic Darlington pair. Hence, we envision that we may readily adapt the intermediate bath formalism we developed in this work to translate a wide variety of useful electronic multitransistor configurations to their thermal equivalents.

DOI: 10.1103/PhysRevB.104.045405

I. INTRODUCTION

Recent years have witnessed significant developments in engineering individual quantum systems that manipulate optical, electrical, and thermal energy in the nanoscale. These technologies have found wide-ranging applications and are currently revolutionizing a variety of fields including electronics [1,2], plasmonics [3–8], photonics [9–11], and medicine [12].

Quantum thermal management involves nanoscale devices and materials which transport, amplify, and control the flow of thermal energy [13]. Strong interest in this area in the last decade has seen the development of thermal rectifiers [14–16], thermal transistors [16–24], optically controlled thermal gates [25,26], and refrigerators [27,28], all fundamentally based on quantum phenomena. Many experimental realizations of these devices have been proposed using quantum dots, metal nanoparticles, and superconducting circuits [17,29,30].

The thermal rectifiers and transistors mentioned above are similar in behavior to their analogous electronic counterparts, with temperatures replacing voltages and thermal energy flows replacing electric currents. Accordingly, a thermal rectifier conducts heat under a particular temperature gradient but acts like a thermal insulator when the gradient is reversed. Similarly, a thermal transistor regulates the heat flow between two of its terminals in response to the temperature of its third terminal.

Over the years, a wide variety of simple quantum thermal systems exhibiting transistor-action have been identified. For instance, Joulain *et al.* [17] and Mandarino *et al.* [23] demonstrated such behaviors in three strongly coupled two-level systems (TLSs) interacting with three external thermal baths. Guo *et al.* [20] identified transistor-action in a similar three-qubit system under trilinear qubit interactions. Zhang *et al.* [21,22] demonstrated that a system of three Coulomb coupled quantum dots can also manifest these behaviors. A different device made of a coupled qubit and qutrit has been shown to also exhibit transistor-action in the thermal domain in Ref. [19]. Majland *et al.* [29] further developed this abstract theoretical model towards a concrete realization using superconducting circuits. The recent work in Wijesekara *et al.* [25] expanded and improved the device in Ref. [17] to allow an external optical field to control the transistor-action. Similar optical control of thermal flows was achieved in Ref. [26] using only a single qubit coupled to two thermal baths, albeit with a significantly reduced control range and efficiency.

The electronic transistor has managed to revolutionize almost all areas of modern technology in a few short decades.

*ravi.wijesekara@monash.edu
†malin.premaratne@monash.edu

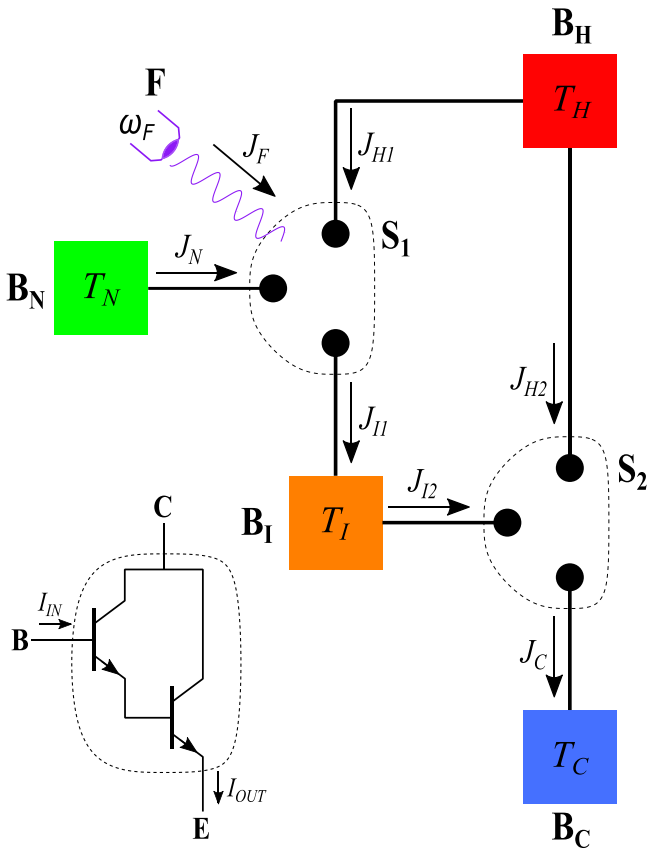

FIG. 1. The system consists of two quantum thermal transistors [17] S_1 and S_2 interconnected in a Darlington configuration. Each thermal bath B_P (where $P = \{H, N, I, C\}$) is characterized by its temperature T_P. The external optical field F on S_1 allows for optical control of the heat flows if necessary [25]. The energy flow rates between the baths B_P (or optical field F) and the quantum transistors are represented by the Js in the directions specified. (Inset) Block diagram of an electronic Darlington pair built using BJTs.

A principal reason for this success was the capability of multiple transistors when combined appropriately, to form composite structures with enhanced transistor-action or even entirely different behaviors. For instance, connecting two electronic transistors as shown in the inset of Fig. 1 creates a configuration commonly known as the Darlington pair [31]. This arrangement multiplies the individual transistors' current gains and builds a composite amplifier with a far superior current gain than either of the constituent devices. Alternative configurations of two transistors can create various other useful devices like logic gates, oscillators, and latches [32]. Integrating many transistors in different configurations has led to the development of arithmetic elements, memory elements, and many other devices that modern electronics thrive on.

It is not immediately obvious whether the above integration capability of electronic transistors is still present in their thermal counterparts. That is, whether a thermal multitransistor system built imitating a particular electronic transistor configuration will have the same behaviors as expected from the original design. The primary reason for this doubt is that handling transistor-transistor interactions in quantum thermal systems is not as simple as in electronics. To elaborate, all previous models for individual thermal transistors had assumed that their terminals' temperatures are held constant despite the thermal flows through the device. However, in a multitransistor system, the temperature of internal transistor interconnects depend mainly on the thermal flow characteristics of the individual transistors and cannot be similarly fixed. Hence, to properly handle these systems, we need to refine and upgrade previous models to allow for varying temperatures and identify mechanisms that properly mediate the thermal energy exchange through internal transistor interconnects. Subsequently, we must verify through numerical simulations whether these systems perform similarly to their electronic counterparts.

In this work, as a first step towards building multitransistor thermal systems, we investigate the Darlington configuration of two quantum thermal transistors. We choose this particular configuration because it showcases the crucial interactions at the internal transistor interconnects well while also being simple enough to analyze and understand quickly.

This paper is organized as follows. In Sec. II, we introduce our Darlington transistor system and review the two models [17,25] we employ to characterize the individual transistors. These two models allow each transistor to be controlled either by a temperature or by an external optical field. We then introduce our model for the internal interconnect between the transistors and further discuss our method's limitations, advantages, and disadvantages. We conclude this section by presenting a unified model for the whole Darlington system. In Sec. III, we numerically simulate both our temperature-controlled and optically controlled Darlington systems using MATHEMATICA™. We provide codes for these simulations in Ref. [33]. We compare the energy flow behaviors of our Darlington pairs with those of corresponding single transistor devices. We thereby demonstrate that the thermal Darlington pairs are analogous to their electronic counterparts under our intermediate bath method. In Sec. IV, we discuss the underlying mechanisms that generate these transistor behaviors and the role our intermediate bath plays in facilitating the thermal energy exchange between the two transistors. Finally, we summarize our results and present our conclusions in Sec. V.

II. MODEL

In this work, we analyze the thermal flow control action of a pair of quantum thermal transistors arranged in a Darlington configuration [31]. In electronics literature, this configuration is used ubiquitously to achieve greater amplification factors and higher input impedances than is possible with a single transistor.

In an electronic Darlington pair built using two NPN bipolar junction transistors (BJTs), the emitter of the first transistor is directly connected to the base of the second transistor, while the collectors of both transistors are connected to the same fixed voltage source as shown in the inset of Fig. 1. The electric current that needs amplification is fed into the base terminal of the first transistor, while the output current is taken out from the emitter terminal of the second transistor. This configuration ensures that the current amplification of the first transistor is compounded with that of the second. The whole two transistor setup is typically grouped and analyzed together

as a single three terminal device, which performs similarly to a single transistor with far superior current gain.

Drawing inspiration from the electronic Darlington pair, our quantum thermal system is arranged as shown in Fig. 1. The three external thermal baths B_H, B_N, and B_C performs analogously to the collector, base, and emitter terminals respectively of the electronic Darlington pair. The temperatures T_P and energy flow rates J_P correspond respectively to voltages and currents in the electronic case. Naturally, the quantum thermal transistors S_1 and S_2 then map to the corresponding electronic transistor pair.

We employ models developed by Joulain *et al.* [17] and Wijesekara *et al.* [25] to calculate the thermal flow rates in each of these individual transistors. We shall discuss the details of these devices extensively in the next section. For now, it suffices to say that these three-terminal devices enable controlling the heat flow rate through their top and bottom (as in Fig. 1) terminals, in response to either the temperature of the middle terminal [17], or the intensity of a properly tuned optical field F incident upon the device [25].

The expected functionality of this composite system would be to control the heat flow rate between B_H and B_C, in response to either the temperature of the control thermal bath B_N, or the strength of the control optical field F. Naturally, the temperature T_H of the bath B_H has to be higher than that of B_C, so that the thermodynamic tendency is for energy to flow from B_H to B_C. However, the magnitude of that heat flow depends upon the effective conductivity of the intermediate device, which we control using one of the mechanisms mentioned above.

In the electronic case, the two transistors can be coupled directly to each other by simply using an electrically conducting wire to connect the two terminals. However, we found that directly coupling the two quantum thermal transistors with a simple interaction Hamiltonian will not achieve the expected result. As we shall see in Sec. IV, the energy flow between the two transistors would be significantly attenuated under a direct coupling because the energy levels associated with the quantum energy exchange between the donor system S_1 and the recipient system S_2 is completely off-resonant. To facilitate an efficient thermal energy transport through this intermediate connection, it is hence necessary to have another quantum system between the two transistors to bridge this gap in energy levels.

In this work, we model this intermediate quantum system as another thermal bath B_I. We will discuss the consequences of this choice, as well as other viable alternatives in Sec. II B. Clearly, the temperature T_I of this intermediate bath is determined by the internal dynamics of the individual transistors, and is therefore not a free parameter of the model. This is analogous to how the voltage of the intermediate terminal of an electronic Darlington pair is not solely set by the external bias, but depends also on the internal electric currents through the individual transistors.

A. Modelling individual thermal transistors

The quantum thermal transistor model we use in this work was first developed by Joulain *et al.* [17], and was subsequently extended by Wijesekara *et al.* [25]. The basic model in [17] introduced a quantum device made up of three strongly-coupled TLSs, denoted L, M, and R. These TLSs respectively interacted with three thermal baths B_L, B_M, and B_R with temperatures T_L, T_M, and T_R. Once the quantum system parameters were properly set and the temperatures biased such that $T_L > T_R$, the device was capable of controlling the heat flow rate from B_L to B_R based on the temperature T_M of the middle thermal bath. Increasing this temperature drastically increased the heat flow rate through the device, effectively exhibiting a transistor-action on the thermal flows.

The extension by Wijesekara *et al.* [25] added an external coherent optical field F with frequency ω_F incident upon the device. By properly tuning the frequency and intensity of the field, the optical interaction between the field and the TLSs could be made to closely emulate the action of a high temperature at B_M. This modified the previous temperature-controlled device into an optically controlled device, in that the thermal flow rate from B_L to B_R was now regulated in response to the strength of the optical field F. Following electronics terminology, this new device was named an optically controlled quantum thermal gate. The maximum possible heat flows of the new device was several times larger than that of the previous, though the energy efficiency was considerably lower.

In this work, we employ the model developed in Ref. [25] to characterize our individual transistors S_1 and S_2, since the former model in Ref. [17] happens to be just a special case of this when the optical field driving strength is set to zero. That aside, we do note that there are other quantum thermal transistor models developed in literature using different base components [19,29] or different interactions [16,20–22,26]. Nevertheless, we believe that the intermediate bath method we employ here can be easily adapted for those models too to obtain similar results.

1. Deriving the Hamiltonian

Following Wijesekara *et al.* [25], each transistor is built from three quantum TLSs, each of which can have one of two possible quantum states, $|\uparrow_Q^S\rangle$ or $|\downarrow_Q^S\rangle$ for $Q = \{L, M, R\}$ and $S = \{S_1, S_2\}$. The full Hilbert space of each device is spanned by the tensor product space of these three individual TLSs, resulting in a combined quantum system with eight eigenstates. These states are given by the eight possible kets of the form

$$|\updownarrow_1\updownarrow_2\updownarrow_3{}^S\rangle = \left|\updownarrow_{1_L}^S\right\rangle \otimes \left|\updownarrow_{2_M}^S\right\rangle \otimes \left|\updownarrow_{3_R}^S\right\rangle, \tag{1}$$

where $\updownarrow = \{\uparrow, \downarrow\}$. For ease of notation we enumerate these eight states

$$\begin{aligned} |1^S\rangle &= |\uparrow\uparrow\uparrow^S\rangle, & |5^S\rangle &= |\downarrow\uparrow\uparrow^S\rangle, \\ |2^S\rangle &= |\uparrow\uparrow\downarrow^S\rangle, & |6^S\rangle &= |\downarrow\uparrow\downarrow^S\rangle, \\ |3^S\rangle &= |\uparrow\downarrow\uparrow^S\rangle, & |7^S\rangle &= |\downarrow\downarrow\uparrow^S\rangle, \\ |4^S\rangle &= |\uparrow\downarrow\downarrow^S\rangle, & |8^S\rangle &= |\downarrow\downarrow\downarrow^S\rangle. \end{aligned} \tag{2}$$

The system Hamiltonian $\hat{H}^S_{\text{sys}}$ of the transistor S is modelled as

$$\hat{H}^S_{\text{sys}} = \frac{\hbar}{2}\big(\omega^S_L\hat{\sigma}^L_z + \omega^S_M\hat{\sigma}^M_z + \omega^S_R\hat{\sigma}^R_z + \omega^S_{LM}\hat{\sigma}^L_z\hat{\sigma}^M_z + \omega^S_{MR}\hat{\sigma}^M_z\hat{\sigma}^R_z + \omega^S_{RL}\hat{\sigma}^R_z\hat{\sigma}^L_z\big), \quad (3)$$

where $\hbar$ is the reduced Planck constant, $\hat{\sigma}^Q$s are the appropriately expanded Pauli matrices [34], $\hbar\omega^S_Q$ is the energy difference between the two eigenstates of the TLS Q, and $\hbar\omega^S_{Q_1Q_2}$ is the interaction energy between the TLSs Q_1 and Q_2 for $Q_1, Q_2 = \{L, M, R\}$. For efficient operation, the system parameters are usually chosen such that $\omega^S_L \approx 0$, $\omega^S_R \approx 0$, $\omega^S_{RL} \approx 0$, and $\omega^S_{LM} \approx \omega^S_{MR} \gg \omega_M \geqslant 0$.

In Eq. (3), the qubit-qubit interactions of the transistor are modelled under an Ising-type $\sigma_z - \sigma_z$ coupling. Under this type of coupling, the system Hamiltonian $\hat{H}^S_{\text{sys}}$ is diagonal in the basis made by the tensor product states in Eq. (1). This ensures that the tensor product states are in fact the energy eigenstates of the quantum transistor. Alternatively, using an Ising-type $\sigma_x - \sigma_x$ coupling would have introduced off-diagonal elements into $\hat{H}^S_{\text{sys}}$, and the eight energy eigenstates would have been superpositions of the tensor product states. However, the transistor-action was demonstrated to persist even under this type of coupling in Mandarino *et al.* [23]. We preferred to employ the $\sigma_z - \sigma_z$ model in this work for its relative mathematical simplicity and intuitive appeal.

The Hamiltonians of the three baths and their interactions with the TLSs of the quantum transistor are characterized according to the Caldeira-Legett model [35] and are respectively given by

$$\hat{H}^{S,Q}_{\text{bath}} = \sum_k \hbar\omega^{S,Q}_k \hat{a}^{S,Q\,\dagger}_k \hat{a}^{S,Q}_k \quad (4)$$

and

$$\hat{H}^{S,Q}_{\text{sys-bath}} = \hbar\hat{\sigma}^Q_x \sum_k g^{S,Q}_k\big(\hat{a}^{S,Q}_k + \hat{a}^{S,Q\,\dagger}_k\big), \quad (5)$$

where k enumerates a large number of thermal bath modes, $\hat{a}^{S,Q}_k$ is the annihilation operator on the bath mode with frequency $\omega^{S,Q}_k$, and $g^{S,Q}_k$ represents the coupling strength between this k^{th} bath mode and the appropriate TLS. Note how these thermal interactions allow each bath to only change the quantum state of the TLS directly linked to it.

The external optical field F is modelled classically with its electric field $\vec{E}^S(t)$ at the device S for time t given by

$$\vec{E}^S(t) = \vec{E}^S_0 \cos\omega^S_F t, \quad (6)$$

where $|\vec{E}^S_0|$ and ω^S_F are respectively its amplitude and frequency. Following the procedure outlined in Ref. [25], we set $\omega^S_F = \omega^S_M + \omega^S_{LM} - \omega^S_{MR} = \omega^S_M - \omega^S_{LM} + \omega^S_{MR}$, and use the dipole approximation to characterize the field-system interaction and the rotating wave approximation (RWA) to further simplify it. We thereby obtain the interaction Hamiltonian between the optical field and the device as

$$\hat{H}^S_{\text{sys-field}}(t) = -\hbar\frac{\Omega^S}{2}\big(|2^S\rangle\langle 4^S| + |4^S\rangle\langle 2^S| + |5^S\rangle\langle 7^S| + |7^S\rangle\langle 5^S|\big) \quad (7)$$

in the interaction picture. Here $\Omega^S = \frac{\vec{E}^S_0\cdot\vec{d}}{\hbar}$ is the Rabi frequency of the optical interaction while $\vec{d}$ is the dipole moment of the TLS used for the dipole approximation above [36]. Because $\Omega^S \propto |\vec{E}^S_0|$ and $\vec{E}^S_0$ represents the strength of the optical field, we identify Ω^S as a measure of the external field's influence on the internal dynamics of the quantum system S. The total Hamiltonian $\hat{H}^S$ of the transistor and its environment now reads

$$\hat{H}^S = \left(\hat{H}^S_{\text{sys}} + \sum_Q \hat{H}^{S,Q}_{\text{bath}}\right) + \left(\hat{H}^S_{\text{sys-field}} + \sum_Q \hat{H}^{S,Q}_{\text{sys-bath}}\right) \quad (8)$$

in the Schrödinger picture. In all subsequent derivations, we work in the interaction picture defined in terms of the first and second terms of the above Hamiltonian.

2. *Lindblad formalism*

Using the well-known Lindblad formalism [34], we can now derive a quantum master equation for the reduced dynamics of the 8×8 density matrix $\hat{\rho}^S(t)$ of the thermal transistor device as

$$\frac{d\hat{\rho}^S(t)}{dt} = -\frac{i}{\hbar}\big[\hat{H}^S_{\text{sys-field}}(t), \hat{\rho}^S(t)\big] + \sum_{Q=L,M,R}\mathcal{L}^S_Q[\hat{\rho}^S(t)] \quad (9)$$

in the interaction picture. The Lindblad superoperator $\mathcal{L}^S_Q[\hat{\rho}]$ which models the influence of bath Q on the transistor S takes the form

$$\mathcal{L}^S_Q[\hat{\rho}] = \sum_{\omega>0}\Big[\mathcal{J}^S_Q(\omega)\big(1+n^S_Q(\omega)\big)\Big(\hat{A}^S_Q(\omega)\hat{\rho}\hat{A}^{S\dagger}_Q(\omega) - \frac{1}{2}\{\hat{A}^{S\dagger}_Q(\omega)\hat{A}^S_Q(\omega), \hat{\rho}\}\Big) + \mathcal{J}^S_Q(\omega)n^S_Q(\omega) \times\Big(\hat{A}^{S\dagger}_Q(\omega)\hat{\rho}\hat{A}^S_Q(\omega) - \frac{1}{2}\{\hat{A}^S_Q(\omega)\hat{A}^{S\dagger}_Q(\omega), \hat{\rho}\}\Big)\Big],$$

where ω runs through all allowed positive energy transitions of the eight-level quantum system and

$$\hat{A}^S_Q(\omega) = \sum_{\epsilon'-\epsilon=\hbar\omega}\hat{\Pi}^S(\epsilon)\hat{\sigma}^Q_x\hat{\Pi}^S(\epsilon') \quad (10)$$

with $\hat{\Pi}^S(\epsilon)$ being the projection of $\hat{H}^S_{\text{sys}}$ towards the eigenvalue ϵ. Note how the $\hat{H}^S_{\text{sys-field}}$ term is not included when defining the projection operators $\hat{\Pi}^S(\epsilon)$. The reasons for this choice will become clearer in the next section when we discuss the underlying assumptions in our models.

The temperature T^S_Q of each thermal bath influences the system dynamics via the distribution function

$$n^S_Q(\omega) = \frac{1}{\exp\left(\frac{\hbar\omega}{k_B T^S_Q}\right) - 1}, \quad (11)$$

where k_B is the Boltzmann constant. The nature of the thermal bath is further characterized through its spectral density function $\mathcal{J}^S_Q(\omega)$. In this work, we consider all baths to be Ohmic with a Lorrentz-Drude cutoff [34,37–39], with the

spectral density

$$\mathcal{J}_Q^S(\omega) = \kappa_Q^S \omega \frac{\omega_{\rm LD}^2}{\omega_{\rm LD}^2 + \omega^2} \tag{12}$$

where $\omega_{\rm LD}$ is the cutoff frequency. Assuming the frequencies of the individual transistors are much smaller than $\omega_{\rm LD}$, we ignore the Lorrentz-Drude cutoff factor and obtain

$$\mathcal{J}_Q^S(\omega) = \kappa_Q^S \omega. \tag{13}$$

The parameter κ_Q^S then directly modulates the strength of the external thermal bath's influence on the internal dynamics of the quantum transistor S.

3. Model limitations

In deriving the quantum master equation in Eq. (9) we invoked the Born, Markov and rotating wave approximations [34,37]. Additionally, by ignoring $\hat{H}^S_{\text{sys-field}}$ when formulating the projectors in Eq. (10), we implicitly considered the field-system interactions to be weak enough that our quantum system's eigenstates remain unaffected by the presence of the optical field. The assumptions associated with all these approximations turn out to be crucial in determining the regions of validity of the method we develop to handle multitransistor systems. Hence, at this point, we will briefly discuss the limitations these approximations place upon our model.

The Born approximation assumes that the quantum states of the thermal reservoirs are minimally affected by their interactions with the quantum system. The Markov approximation further assumes that bath correlations die down in timescales τ_B much shorter than the timescales τ_R associated with system density matrix evolution. Finally, when ignoring fast-oscillating terms under the RWA, we implicitly assume that the timescales τ_S associated with transitions between energy eigenstates of the quantum system are much shorter than τ_R [34].

It is generally understood that to satisfy these conditions, the thermal baths need to have a large (ideally infinite) number of harmonic oscillator modes and a weak system-bath coupling [40]. This effectively means that the thermal baths have to be physically large enough to supply the heat flows to the quantum system without significantly affecting their own thermal properties. Since our model for the Darlington pair introduces an intermediate thermal bath B_I which is internal to the device, this will place limitations on both the physical size of the device as well as its speed of operation. We will discuss these issues in more detail in Sec. II B.

Since the system-bath couplings are represented in the master equation by the spectral densities $\mathcal{J}_Q^S(\omega)$, we can reformulate the above weak coupling condition as

$$\Delta \gg \mathcal{J}_Q^S(\Delta), \tag{14}$$

where Δ represents the frequency scale associated with the eigenvalues of $\hat{H}^S_{\rm sys}$ [26,40,41]. For the specific case of Ohmic baths, this condition simplifies to $1 \gg \kappa_Q^S$.

We introduced the optical interaction in Eq. (7) to support and enhance some of the thermally induced mechanisms already present in the temperature-controlled version of the transistor [17]. As such, we do not require the strength of this optical interaction to go significantly beyond the strength of the original transistor's thermal interactions. Numerically, this means that the scale of Ω^S need only be large as the scale of $\mathcal{J}_Q^S(\Delta)$ for our purposes. Together with our earlier condition in Eq. (14), this results in

$$\Delta \gg \Omega^S. \tag{15}$$

As it happens, this condition essentially means that the optical driving is not strong enough to significantly change the energy levels or the thermal dissipation mechanisms of the quantum system. We can easily verify this by noting that $\hbar\Delta$ and $\hbar\Omega^S$ represent the energy scale of $\hat{H}^S_{\rm sys}$ and $\hat{H}^S_{\text{sys-field}}$ respectively. This allows us to follow the paradigmatic strategy for deriving the optical Bloch equations [42] and ignore the effects of $\hat{H}^S_{\text{sys-field}}$ when formulating the Lindblad superoperators for the master equation. Ultimately, even though Eq. (15) came about from us not needing too strong of an optical drive, it nonetheless places an upper bound on how strong the drive can be before our model starts getting inaccurate.

4. Dynamics of the density matrix

The reduced dynamics of our quantum thermal device can be obtained by solving the master equation in Eq. (9) along with the necessary initial conditions. Since $\hat{\rho}^S(t)$ is an 8×8 matrix, we will have a system of 64 coupled first-order differential equations to solve.

Luckily, the differential equations governing most of the off-diagonal density matrix elements will have a form that will ensure they eventually decay to zero irrespective of the initial conditions. The only four off-diagonal elements to not do so will be those under the influence of the external field F as given in Eq. (7). The equations for these four density matrix elements can be written in the compact form

$$\begin{aligned}
\dot{\rho}^S_{24} &= \gamma^S_{42} - \frac{1}{2}\big(\beta^{S,L}_{62} + \beta^{S,L}_{84} + \alpha^{S,M}_{42} \\
&\quad + \beta^{S,M}_{42} + \alpha^{S,R}_{21} + \alpha^{S,R}_{43}\big)\rho^S_{24}, \\
\dot{\rho}^S_{42} &= \gamma^S_{24} - \frac{1}{2}\big(\beta^{S,L}_{62} + \beta^{S,L}_{84} + \alpha^{S,M}_{42} \\
&\quad + \beta^{S,M}_{42} + \alpha^{S,R}_{21} + \alpha^{S,R}_{43}\big)\rho^S_{42}, \\
\dot{\rho}^S_{57} &= \gamma^S_{75} - \frac{1}{2}\big(\alpha^{S,L}_{51} + \alpha^{S,L}_{73} + \alpha^{S,M}_{75} \\
&\quad + \beta^{S,M}_{75} + \beta^{S,R}_{65} + \beta^{S,R}_{87}\big)\rho^S_{57}, \\
\dot{\rho}^S_{75} &= \gamma^S_{57} - \frac{1}{2}\big(\alpha^{S,L}_{51} + \alpha^{S,L}_{73} + \alpha^{S,M}_{75} \\
&\quad + \beta^{S,M}_{75} + \beta^{S,R}_{65} + \beta^{S,R}_{87}\big)\rho^S_{75},
\end{aligned} \tag{16}$$

where

$$\begin{aligned}
\alpha^{S,Q}_{jk} &= \mathcal{J}^S_Q\big(\omega^S_{jk}\big)\big(1 + n^S_Q\big(\omega^S_{jk}\big)\big), \\
\beta^{S,Q}_{jk} &= \mathcal{J}^S_Q\big(\omega^S_{jk}\big) n^S_Q\big(\omega^S_{jk}\big), \\
\gamma^S_{jk} &= i\frac{\Omega^S}{2}\big(\rho^S_{jj} - \rho^S_{kk}\big),
\end{aligned} \tag{17}$$

and $\hbar\omega^S_{ij} = \hbar(\omega^S_i - \omega^S_j)$ represents the energy difference between the $i^{\rm th}$ and $j^{\rm th}$ eigenstates of the system Hamiltonian, $\hat{H}^S_{\rm sys}$. Here we have not indicated the explicit time dependence of the density matrix elements for clarity.

Note how these off-diagonal elements are prevented from decaying to zero by the γ_{jk}^S terms, which in turn depend upon the driving strength Ω^S of the optical field. To get the more restricted quantum transistor model of Ref. [17], we can simply set $\Omega^S = 0$, in which case these four off-diagonal elements decay to zero just like all the others. This would correspond to the situation where the optical field F is absent and $|\vec{E}_0^S| = 0$.

On the other hand, the equations for the eight diagonal elements of the density matrix simplify to

$$\begin{aligned}
\dot{\rho}_{11}^S &= +\Gamma_{51}^{S,L} + \Gamma_{31}^{S,M} + \Gamma_{21}^{S,R},\\
\dot{\rho}_{22}^S &= +\Gamma_{62}^{S,L} + \Gamma_{42}^{S,M} - \Gamma_{21}^{S,R} - \Upsilon_{24}^S,\\
\dot{\rho}_{33}^S &= +\Gamma_{73}^{S,L} - \Gamma_{31}^{S,M} + \Gamma_{43}^{S,R},\\
\dot{\rho}_{44}^S &= +\Gamma_{84}^{S,L} - \Gamma_{42}^{S,M} - \Gamma_{43}^{S,R} + \Upsilon_{24}^S,\\
\dot{\rho}_{55}^S &= -\Gamma_{51}^{S,L} + \Gamma_{75}^{S,M} + \Gamma_{65}^{S,R} - \Upsilon_{57}^S,\\
\dot{\rho}_{66}^S &= -\Gamma_{62}^{S,L} + \Gamma_{86}^{S,M} - \Gamma_{65}^{S,R},\\
\dot{\rho}_{77}^S &= -\Gamma_{73}^{S,L} - \Gamma_{75}^{S,M} + \Gamma_{87}^{S,R} + \Upsilon_{57}^S,\\
\dot{\rho}_{88}^S &= -\Gamma_{84}^{S,L} - \Gamma_{86}^{S,M} - \Gamma_{87}^{S,R},
\end{aligned} \tag{18}$$

where

$$\Gamma_{jk}^{S,Q} = \mathcal{J}_Q^S\big(\omega_{jk}^S\big)\Big(\big(1 + n_Q^S\big(\omega_{jk}^S\big)\big)\rho_{jj}^S - n_Q^S\big(\omega_{jk}^S\big)\rho_{kk}^S\Big) \tag{19}$$

represents the transition rate from state $|j\rangle$ to state $|k\rangle$ induced by the system-bath thermal interactions, and

$$\Upsilon_{jk}^S = i\frac{\Omega^S}{2}\big(\rho_{jk}^S - \rho_{kj}^S\big) \tag{20}$$

represents the transition rate from state $|j\rangle$ to state $|k\rangle$ induced by the system-field optical interaction.

Solving this set of 12 first-order differential equations along with the probability condition

$$\mathrm{Tr}\{\hat{\rho}^S\} = \sum_{j=1}^{8} \rho_{jj}^S = 1, \tag{21}$$

where $\mathrm{Tr}\{\hat{X}\}$ denotes the matrix trace, allows us to fully specify the density matrix evolution of the optically controlled quantum gate developed in Ref. [25] from any initial condition. Setting $\Omega^S = 0$ and dropping the off-diagonal equations allows the same for the quantum thermal transistor developed in Ref. [17].

Once the density matrix $\hat{\rho}^S(t)$ at any given time t is known, the expected value of any other observable $\hat{A}(t)$ at the same time can be easily calculated through the elementary formula,

$$\langle \hat{A}^S(t)\rangle = \mathrm{Tr}\{\hat{A}^S(t)\hat{\rho}^S(t)\}. \tag{22}$$

5. Calculating thermal flows

Our analysis of these quantum devices in this work is fundamentally based on the energy flow rates to and from the different components of each quantum system. To obtain expressions for these flow rates, we employ the principle of energy conservation in the following way.

Since energy is always conserved, the rate of change of the internal energy of any classical system has to equal its net energy inflow from external sources. Incidentally, this is simply a statement of the first law of thermodynamics. When quantum systems are concerned, these exact quantities are simply replaced by their corresponding expected values. When applied to our quantum transistor S, this leads to the continuity equation [15]

$$\begin{aligned}
J_F^S(t) + \sum_{Q=L,M,R} J_Q^S(t) &= \frac{\partial\langle \hat{H}_{\mathrm{sys}}^S\rangle}{\partial t}\\
&= \mathrm{Tr}\left\{\hat{H}_{\mathrm{sys}}^S \frac{d\hat{\rho}^S(t)}{dt}\right\},
\end{aligned} \tag{23}$$

where J_F and J_Q denote the net energy inflows to the system from the optical field and thermal bath Q respectively.

By using the master equation to substitute for $\frac{d\hat{\rho}^S(t)}{dt}$ and comparing similar terms we obtain the following expressions for the energy inflows [15,17,25]

$$\begin{aligned}
J_F^S &= -\big(\epsilon_{24}^S\Upsilon_{24}^S + \epsilon_{57}^S\Upsilon_{57}^S\big),\\
J_L^S &= -\big(\epsilon_{51}^S\Gamma_{51}^{S,L} + \epsilon_{62}^S\Gamma_{62}^{S,L} + \epsilon_{73}^S\Gamma_{73}^{S,L} + \epsilon_{84}^S\Gamma_{84}^{S,L}\big),\\
J_M^S &= -\big(\epsilon_{31}^S\Gamma_{31}^{S,M} + \epsilon_{42}^S\Gamma_{42}^{S,M} + \epsilon_{75}^S\Gamma_{75}^{S,M} + \epsilon_{86}^S\Gamma_{86}^{S,M}\big),\\
J_R^S &= -\big(\epsilon_{21}^S\Gamma_{21}^{S,R} + \epsilon_{43}^S\Gamma_{43}^{S,R} + \epsilon_{65}^S\Gamma_{65}^{S,R} + \epsilon_{87}^S\Gamma_{87}^{S,R}\big),
\end{aligned} \tag{24}$$

where $\epsilon_{ij}^S = \hbar\omega_{ij}^S$ represents the energy level difference between the eigenstates $|i\rangle$ and $|j\rangle$.

The Eqs. (16), (18), (21), and (24), along with some initial conditions, form our model for analyzing the time-dependent thermal behavior of any individual thermal transistor. For our Darlington pair shown in Fig. 1, if the temperatures T_H, T_N, T_I, T_C, and optical field strength Ω_F is known, we can use these equations to find the heat flow rates through each of the thermal transistors S_1 and S_2 starting from any initial density matrix. However, since the temperature T_I of the intermediate bath happens to depend on the internal heat flows and is initially unknown, we cannot fully solve the system just utilizing the individual transistor models alone.

B. Modelling the intermediate thermal bath

In earlier work on individual quantum transistors [17,19,21,25,29], it was always assumed that the temperatures of the external thermal baths were held constant at predetermined values. This meant that the thermal baths were either physically so large that the heat flows J_Q in to the thermal transistor hardly affected their temperatures, or that they had other unmodelled interactions which maintained the bath temperature in spite of these flows. In simple terms, the analysis did not consider how the heat flows might raise or lower the temperature of the thermal bath. Nevertheless, this did not affect the validity of the thermal analysis since the thermal baths were anyway external to the system of interest.

In our Darlington pair system, the external thermal baths B_H, B_N, and B_C certainly comply with the above assumptions. However, the intermediate thermal bath B_I is completely internal to the system under analysis and its temperature depends upon the thermal flow rates of the individual transistors. Hence, to model the thermal behaviors of B_I, we first need to find the relationship between its temperature T_I and its average internal energy E_{int}^I. We can subsequently invoke the principle

of energy conservation to relate E^I_{int} to the relevant thermal energy flow rates J_{I1} and J_{I2}.

We begin by defining the heat capacity $C_I(T_I)$ of the thermal bath at temperature T_I as

$$C_I(T_I) = \frac{dE^I_{\text{int}}}{dT_I}. \tag{25}$$

Using the previous characterization of the thermal bath in Eq. (4) as an ensemble of quantum harmonic oscillators, we can derive a theoretical expression for $C_I(T_I)$ following the procedure outlined in the Appendix. Alternatively, for a particular experimental realization of the intermediate thermal bath, a more phenomenological expression for the heat capacity may be obtained by considering its physical and material properties. After $C_I(T_I)$ is fully characterized using either method, the internal energy-temperature relationship of the thermal bath may be obtained by integrating Eq. (25).

As energy is conserved within B_I, the rate of change of its average internal energy must equal the sum of its thermal flow rates coming inwards from external sources, resulting in the continuity equation

$$\frac{dE^I_{\text{int}}}{dt} = J_{I1} - J_{I2}. \tag{26}$$

Here J_{I1} is the energy flow rate from S_1 to B_I, and J_{I2} is the energy flow rate from B_I to S_2 as shown in Fig. 1.

Combining Eq. (25) with Eq. (26) gives us the complete model for characterizing the thermal behaviors of the intermediate bath as

$$J_{I1} - J_{I2} = \frac{dE^I_{\text{int}}}{dT_I}\frac{dT_I}{dt} = C_I(T_I)\frac{dT_I}{dt}. \tag{27}$$

The temperature of B_I now varies with time, depending upon the difference between the heat flows towards the two thermal transistors.

1. Model limitations

Before further analysis, it is important first to discuss the assumptions employed while deriving Eq. (27) and the physical conditions required for them to remain valid.

First of all, depending on the nature of the thermal bath, its heat capacity C_I may or may not depend upon its temperature. However, most of our simulations in Sec. III will be concentrating on the steady-state condition of our Darlington pair system, after any transients due to an unbalanced initial state have died out. Since $\frac{dT_I}{dt} = 0$ anyway at the steady state, the exact value of C_I (or its temperature dependence behavior) will not affect the steady-state solutions at all.

As we shall find in Sec. III B, the system will eventually relax to this steady state regardless of the initial conditions as long as the internal energy of the bath is an increasing function of its temperature [i.e., $C_I(T_I) > 0$], which is proven in the Appendix to be always true. This is further clarified by the fact that almost all known physical materials have positive heat capacities [43].

Even though the final steady state is independent of C_I, it still determines the relaxation path the system follows to reach that steady state. When we study the relaxation behaviors of our system in Sec. III D, we will be assuming that C_I is independent of T_I for simplicity. According to our discussion in the Appendix, this assumption will be reasonable if the thermal bath B_I mainly contains low-frequency harmonic oscillators.

As discussed previously in Sec. II A 3, allowing B_I to have a finite heat capacity (and hence a finite physical size) could affect the Born-Markov approximations used in deriving the individual transistor models. For instance, an undersized bath may mean that not enough bath oscillators are leftover in B_I to properly manifest Markovian dynamics. We refer the interested reader to Rivas *et al.* [40] and Hofer *et al.* [41] for an in-depth discussion on the validity of Born-Markov master equations when the number of bath oscillators is finite.

To employ models developed assuming temperatures are constant in a situation where they are actually changing, we have to at least make sure that the timescale τ_T over which a significant change in T_I is observed is much longer than the timescale τ_R associated with the thermal relaxation of an individual transistor [i.e., $\tau_T \gg \tau_R$]. This condition will justify a variant of the adiabatic approximation on each quantum transistor. In simple terms, the previous model with fixed temperatures can still be assumed valid because the temperatures change only slightly in the timescale over which the individual transistor operates.

By inspection, from Eq. (27), we can write an approximate expression for the timescale τ_T as

$$\tau_T \approx C_I(T_I)\frac{\Delta T_I}{J_{I1} - J_{I2}}, \tag{28}$$

where ΔT_I represents a small change in the temperature of T_I. On the other hand, τ_R can be approximated by numerically simulating an individual quantum transistor and measuring the time it takes to reach its steady state. The condition $\tau_T \gg \tau_R$ will then become an approximate minimum bound on the heat capacity C_I of the intermediate bath.

2. Model advantages and disadvantages

Unfortunately, the above $\tau_T \gg \tau_R$ condition means that the time it takes for the Darlington transistor pair to reach its steady state will be considerably longer than that of a single thermal transistor. In electronics terminology, the switching speed of the thermal Darlington pair will be considerably slower. In a broader context, this would be the main disadvantage in almost every situation where we employ intermediate baths for handling multitransistor systems.

On the other hand, the advantages of using this method are numerous. First, the introduction of intermediate baths divides the multitransistor system into blocks that can be analyzed individually using existing models. Second, this separability makes the method scalable for handling systems made up of a large number of transistors. In contrast, any method that analyzes multiple quantum transistors together experiences an exponential increase of simulation complexity due to the tensor products involved when combining different Hilbert spaces. For example, combining two quantum transistors with 8-dimensional Hilbert spaces each would result in a 64-dimensional compound Hilbert space. Since the number of density matrix elements further squares the dimensionality of the Hilbert space, the lack of computational scalability is obvious. Thirdly, the conditions required of a thermal bath

are generally easier to realize in physical systems than other intermediary quantum systems (such as harmonic oscillators), which generally needs careful tuning.

We finally note that there are nevertheless other quantum systems that can act as intermediaries between two thermal transistors. In fact, a single properly tuned quantum harmonic oscillator or multilevel system shows promise in mediating these interactions. However, since their theoretical treatment is quite different from the method employed here, we will present them separately in a future paper.

C. Combined system model

With the models for the individual components of the Darlington pair system completely specified, we can begin analyzing and simulating the dynamics of the full system. Since we have both the temperature-controlled [17] and optically controlled [25] versions for the individual transistors, we can build two different composite systems.

If we are interested in building a Darlington pair controlled by the temperature T_N of the control bath B_N, both transistors need to be modelled after [17]. Setting $\Omega^S = 0$ in Eq. (18) and ignoring Eq. (16), we will end up with 2×8 equations governing the dynamics of S_1 and S_2. Together with Eqs. (21) and (27), this results in a set of 17 independent first-order differential equations. We can numerically solve these equations to obtain the time-evolution of the Darlington pair system from any initial condition. As we shall see in next few sections, once we fix T_H at a high temperature and T_C at a low temperature, the thermal energy flow rate between B_H and B_C will be controllable through appropriately adjusting T_N.

On the other hand, a Darlington pair incorporating an optically controlled transistor modelled after Ref. [25] will have a slightly different configuration. Here, only the first transistor will directly interact with the external field F, while the second transistor will be optically shielded or off-resonant. Hence, the second device will still be a temperature-controlled device as before. Though this system does not match the strictest definition of a Darlington pair, it will still make a compound device which can function with far lower optical field strengths at better efficiency than a single optically controlled transistor. Since the first transistor will now have four nonzero off-diagonal terms as given by Eq. (16), we will have a total of 21 first-order differential equations for solving the dynamics.

We note that there is a third configuration possible where the optical field controls both transistors. However, with the second transistor interacting with the input, this happens to be quite different from a Darlington configuration. Accordingly, we do not analyze this system in the main discussion but make the results available at Ref. [33].

From observing Fig. 1, we can easily map the bath temperatures for S_1 and S_2 as follows:

$$\begin{aligned} T_L^{S_1} &= T_H, & T_L^{S_2} &= T_H, \\ T_M^{S_1} &= T_N, & T_M^{S_2} &= T_I(t), \\ T_R^{S_1} &= T_I(t), & T_R^{S_2} &= T_C. \end{aligned} \tag{29}$$

Consequently, the thermal energy flow rates read

$$\begin{aligned} J_L^{S_1}(t) &= J_{H1}(t), & J_L^{S_2}(t) &= J_{H2}(t), \\ J_M^{S_1}(t) &= J_N(t), & J_M^{S_2}(t) &= J_{I2}(t), \\ J_R^{S_1}(t) &= -J_{I1}(t), & J_R^{S_2}(t) &= -J_C(t). \end{aligned} \tag{30}$$

Since the thermal bath B_H provides thermal flows to both S_1 and S_2, its total flow rate $J_H(t)$ is given by

$$J_H(t) = J_{H1}(t) + J_{H2}(t). \tag{31}$$

For the optically controlled case, we additionally have $\Omega^{S_1} = \Omega_F$, $J_F^{S_1} = J_F$, and $\Omega^{S_2} = 0$. Furthermore, for simplicity we assume all κ_Q^S to be equal

$$\kappa_Q^S = \kappa \tag{32}$$

for $Q = \{L, M, R\}$ and $S = \{S_1, S_2\}$. After specifying numerical values for above temperatures and for transistor parameters ω_Q^S, $\omega_{Q_1Q_2}^S$ we will be in a position to start simulating the Darlington pair system.

III. SIMULATIONS AND RESULTS

In this section, we present and discuss the results obtained from our numerical simulations of Darlington quantum thermal transistor pairs for different system and environment parameters. In all simulations, we work with SI units where the reduced Planck constant is $\hbar = 1.055 \times 10^{-34}$ Js and the Boltzmann constant is $k_B = 1.381 \times 10^{-23}$ J/K.

A. Simulation parameters

The expected functionality of the Darlington pair is to regulate the thermal energy flow from the thermal bath B_H to the thermal bath B_C. As such, their respective temperatures T_H and T_C have to be chosen such that $T_H > T_C$. In the current state-of-the-art, the widest range of experimental technologies for realizing these quantum devices, such as superconducting circuits and circuit quantum electrodynamics, are available at low temperatures [44–46]. In fact, the majority of recent theoretical and experimental work on quantum thermal systems envision their operation at sub-Kelvin temperature ranges [19,21,24,29,47]. Therefore, taking the temperature scale to be in the milli-Kelvin range and the temperature ratio to reflect values commonly used in the literature for individual transistor models [15,17,19,25], we set $T_H = 300$ mK and $T_C = 30$ mK in our simulations. This means that the temperature T_N of the third external bath B_N should vary within the range $T_N = [T_C, T_H] = [30\text{ mK}, 300\text{ mK}]$.

For temperature-based control, T_N will be varied within this full range to regulate the heat flows. For optical control, T_N will instead need to be fixed at some bias temperature beforehand. In our simulations, we choose this bias at $T_N = T_C = 30$ mK. This will ensure that the thermal transistors will be at their least conducting setting when the external optical field is absent [i.e., $\Omega_F = 0$]. Additionally, this bias will be easy to realize by simply connecting or merging the thermal bath B_N with B_C.

Our next task is to specify the parameters ω_Q^S and $\omega_{Q_1Q_2}^S$ of the individual transistors S_1 and S_2. Beforehand, we have to identify the appropriate frequency scale Δ associated with

the transistor energy levels. According to previous studies [15,17,25], Δ depends upon the operating temperatures of the setup through the relation

$$\hbar\Delta \approx 5k_{\mathrm{B}}T. \tag{33}$$

By substituting $T \approx 300$ mK in this equation, the approximate scale for transistor frequencies can be derived as $\Delta \approx 3.12 \times 10^{10}$Hz or $\Delta \approx 1.96 \times 10^{11}\mathrm{rads}^{-1}$.

With the frequency scale properly identified, we are now in a position to fully specify the system parameters of S_1 and S_2. For modeling all temperature-controlled quantum thermal transistors, we will choose these parameters as

$$\begin{aligned} \omega_L^S &= 0, \quad \omega_{LM}^S = 0.9\Delta, \\ \omega_M^S &= 0, \quad \omega_{MR}^S = 1.1\Delta, \\ \omega_R^S &= 0, \quad \omega_{RL}^S = 0. \end{aligned} \tag{34}$$

On the other hand, the same parameters for all optically controlled transistors will be

$$\begin{aligned} \omega_L^S &= 0, \quad \omega_{LM}^S = \Delta, \\ \omega_M^S &= 0.1\Delta, \quad \omega_{MR}^S = \Delta, \\ \omega_R^S &= 0, \quad \omega_{RL}^S = 0. \end{aligned} \tag{35}$$

Furthermore, the bath-system coupling term κ will be taken as

$$\kappa = 0.01 \tag{36}$$

in keeping with our discussion in Sec. II A 3. As mentioned previously, Eq. (34) will model S_2 in the optically controlled Darlington configuration, and both S_1 and S_2 in the temperature-controlled configuration. Eq. (35) will model S_1 in the optically controlled situation.

The optical field strength Ω_F^S will be set to zero for temperature-based control and will be varied as required for optical control. From our simulations, we find that arbitrarily increasing Ω_F^S beyond a certain point will not have much influence on the regulated heat flows. Borrowing electronics terminology, it can be said that the transistor-action will eventually saturate at high optical driving strengths. Identifying from the simulations when this saturation sets in, we will be only varying Ω_F^S within the range $\Omega_F^S = [0, 0.7\kappa\Delta]$. Note that our previous model condition in Eq. (15) is satisfied for this whole Ω_F^S range.

These chosen parameter values demonstrate the relevant thermal regulation behaviors of each transistor type well, while also simplifying the mathematics considerably. It must be said however that the required transistor behaviors are present for a wide range of system parameters, and that these particular values are simply representative. By using different values, different features and characteristics of the transistor, such as the amplification factor, thermal efficiency or maximum possible heat flow, may be optimized. For the interested reader, our MATHEMATICA™ based code in Ref. [33] will allow numerically simulating the Darlington pair for arbitrary sets of system parameters.

B. Existence of steady-state solutions

Previous studies on individual quantum thermal transistors have found that, if the bath temperatures and optical field strengths are held constant, the quantum system always relaxes to a single stationary state from any initial state. Once reaching this state, the elements of the density matrix, as well as the thermal flow rates of the baths, will no longer be varying with time. In fact, it is these steady-state heat flows that demonstrate the reported transistor like behaviors.

It is not immediately obvious that just because individual transistors have a steady-state solution, multitransistor systems like our Darlington pair should have a viable steady state too. In a similar vein, the possibility of multitransistor systems having multiple viable steady states cannot be discounted. Hence, we begin with an investigation on whether there exist steady-state solutions for the Darlington pair system, and if they do, how many there are.

The typical process for finding steady-state solutions starts with fixing all the system and environment parameters, including the control parameters T_N and Ω_F. We then use Eqs. (21), (24), (29), and (30) to substitute in our equations of motion, namely Eq. (27) for the intermediate bath B_I, and Eqs. (16) and (18) for transistors S_1 and S_2. Taking the substituted differential equations, we then assert

$$\frac{d\rho_{ij}^{S_1}(t)}{dt} = 0, \quad \frac{d\rho_{ij}^{S_2}(t)}{dt} = 0, \quad \frac{dT_I(t)}{dt} = 0, \tag{37}$$

and drop any time dependence from the ρ_{ij}^S, T_P and J_P terms. We then solve the resulting equations for T_I, $\rho_{ij}^{S_1}$ and $\rho_{ij}^{S_2}$ to get the steady-state density matrices, and finally use Eq. (24) again to find the steady-state thermal flows.

While these equations are linear in the $\rho_{ij}^{S_1}$ terms, they will have an exponential dependence on T_I due to Eq. (11). This will make it impossible to get a simple analytical solution for the full set of equations. A potential workaround is to initially fix the T_I at a certain value, solve the now linear equations for $\rho_{ij}^{S_1}$ and $\rho_{ij}^{S_2}$, and finally calculate $J_{I1} - J_{I2}$ in Eq. (27) to verify whether $\frac{dT_I}{dt}$ is indeed zero. By sweeping T_I through the thermodynamically allowed range $[T_C, T_H]$, we can find all possible solutions for the steady state.

Conceptually, this is equivalent to solving the transistors S_1 and S_2 individually while artificially holding T_I constant, and verifying whether the heat flows J_{I1} and J_{I2} are equal for that particular T_I. In Fig. 2, we have shown the different values obtained for J_{I1} and J_{I2} while keeping Ω_F and T_N fixed and sweeping T_I through its full range. From the $J_{I1} - J_{I2}$ graph, it is quite obvious that only a single steady-state solution exists for the system, at least within the $T_I = [T_C, T_H]$ range.

Moreover, we can easily observe from Eq. (27) that, since $C_I(T_I) > 0$, positive (negative) values of $J_{I1} - J_{I2}$ tend to increase (decrease) T_I. Together with the shape of the $J_{I1} - J_{I2}$ graph in Fig. 2, this implies that any initial value for T_I eventually drifts to this single steady state as time goes on. The speed of this drift will depend upon the magnitude of the heat capacity C_I of the intermediate thermal bath.

In Fig. 3, we present the steady-state values of T_I obtained while sweeping the control parameters T_N or Ω_F through their full range. In both temperature and optically controlled

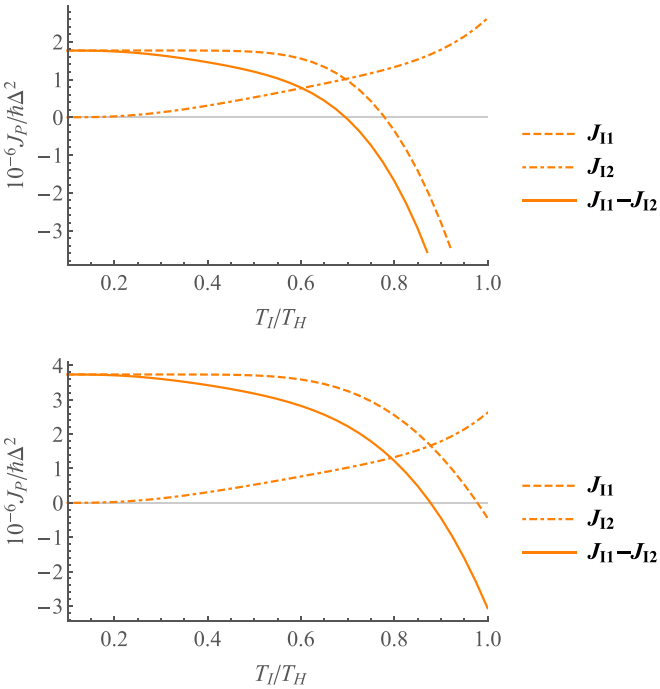

FIG. 2. Steady-state heat flows to and from B_I obtained from individual transistor models when T_I is artificially held constant at different values. (Top) Temperature-controlled configuration for control parameter $T_N = 0.4T_H$. (Bottom) Optically controlled configuration for control parameter $\Omega_F = 0.3\kappa\Delta$. All other parameters are as given in Sec. III A.

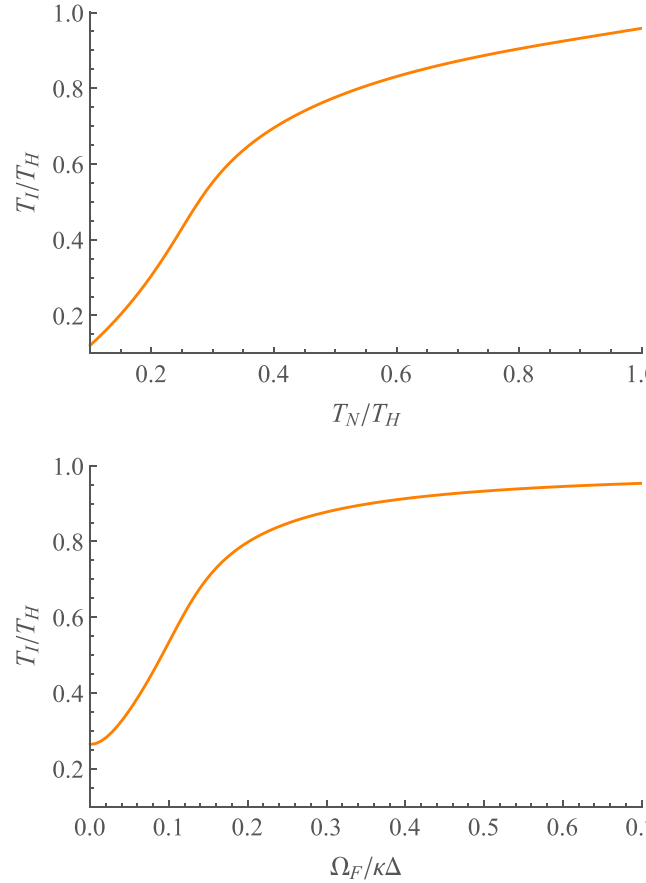

FIG. 3. Steady-state temperature T_I of the intermediate bath B_I for the full control parameter range. (Top) Temperature-controlled configuration while varying T_N within the range $[T_C, T_H]$. (Bottom) Optically controlled configuration while varying Ω_F within the range $[0, 0.7\kappa\Delta]$. All other parameters are as given in Sec. III A.

situations, we see that a small increase in the input signal leads to a significantly larger temperature increase for B_I. In brief, the second transistor experiences a strongly amplified version of the initial input signal. Therefore it is natural for the amplification factor of a thermal Darlington pair to be significantly higher than that of a single transistor.

C. Thermal flow rates in the steady state

In the previous section, we established that the Darlington transistor pair has only a single steady state, and that any initial state eventually converges to that particular steady state as long as the external environmental parameters are held constant. Now we move on to analyzing these steady-state energy flow behaviors in more detail.

For our analysis, we can think of the whole Darlington transistor pair as a single three terminal device. Depending on the control mechanism, either T_N or Ω_F can act as the input signal, while the energy flow rates J_N or J_F correspondingly make up the input "current." For both mechanisms, the energy flow rates J_H and J_C constitute the regulated output "current."

1. Temperature-based control mechanism

In Fig. 4, we present the steady-state operating characteristics of a Darlington pair with a temperature-based control mechanism. The control parameter T_N is varied in the range $[T_C, T_H]$, and the corresponding input thermal flow J_N and output thermal flows J_C and J_H are recorded. We compare these characteristic curves with those obtained by replacing the Darlington pair with a single quantum thermal transistor whose system parameters are given by Eq. (34).

We observe that increasing the input temperature T_N results in a corresponding increase of the output flows J_C and J_H. The input thermal flow J_N consumed by the device for this control action is over a order of magnitude smaller than the regulated thermal flows. Hence, it is quite obvious that our Darlington pair performs as a high gain amplifier on the thermal energy flows.

Compared to the single transistor, our Darlington pair achieves higher output thermal flows while consuming far lower input thermal flows for the whole temperature range. Moreover, these high output flows are achieved at significantly lower control temperatures. In short, the Darlington system exhibits superior thermodynamic efficiency as well as superior sensitivity.

To further clarify these comparisons, we define the thermal flow amplification factor $\beta_{\rm Te}$ and temperature sensitivity factor $\eta^P_{\rm Te}$ for our devices as

$$\beta_{\rm Te} = \frac{J_H}{J_N}, \quad \eta^P_{\rm Te} = \frac{\partial J_P}{\partial T_N}. \tag{38}$$

Since $\beta_{\rm Te}$ measures the regulated thermal flow in terms of the input thermal flow, it also represents the thermal efficiency

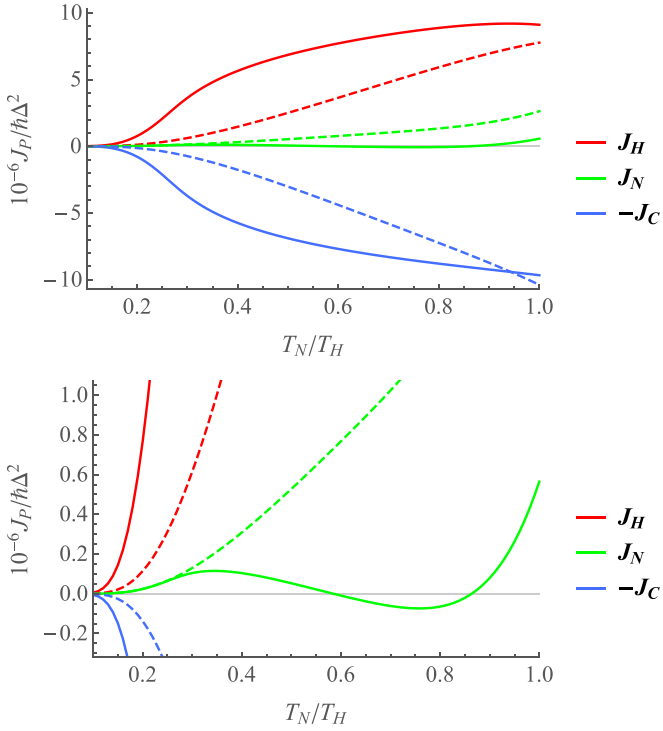

FIG. 4. (Solid) Overall steady-state energy flow rates for the external thermal baths B_H, B_N, and B_C of the temperature-controlled configuration of the Darlington pair system for $T_N = [T_C, T_H]$ range. (Dashed) For comparison, the same figures if the Darlington pair is replaced with a single temperature-controlled thermal transistor [17]. All simulation parameters are as given in Sec. III A.

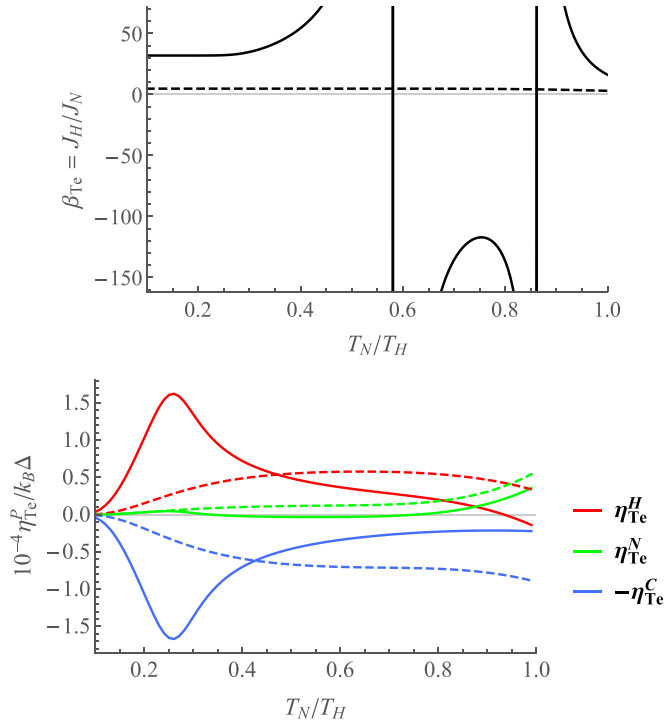

FIG. 5. (Solid) Thermal flow amplification factor $\beta_{\rm Te}$ and thermal flow sensitivity factor $\eta^P_{\rm Te}$ for the temperature-controlled configuration of the Darlington pair system for $T_N = [T_C, T_H]$ range. (Dashed) For comparison, the same figures if the Darlington pair is replaced with a single temperature-controlled thermal transistor [17]. All simulation parameters are as given in Sec. III A.

of the device. On the other hand, $\eta^P_{\rm Te}$ measures how sensitive each thermal flow is to a slight increase in the input temperature. Higher values of $\eta^P_{\rm Te}$ generally indicate a superior amplification action. In the electronic case, a Darlington configuration is typically expected to square the amplification factor of a single device [32].

From Fig. 5, we can observe that $\beta_{\rm Te}$ is always significantly larger in the Darlington pair compared to the single transistor. Even in the low-temperature regime, the expected amplification factor squaring is actually surpassed. Interestingly, the thermal flow amplification becomes negative in the $T_N \approx [0.6T_H, 0.85T_H]$ region, meaning that the device is actually forcing energy backwards out of the input terminal. This behavior is not uncommon for certain configurations of these thermal devices [17,19]. After all, since $T_H > T_N$ such flows are not thermodynamically forbidden.

Figure 5 also shows that the sensitivity factors $\eta^P_{\rm Te}$ taper off in the high temperature regime for both devices. This saturation effect commonly emerges when the thermal flows approach the maximum capacity of the amplifying device. Since the Darlington pair naturally has higher thermal flows and amplification, saturation is reached at a comparatively low temperature.

All these results agree that the Darlington thermal transistor pair has superior thermal flow amplification, sensitivity and thermodynamic efficiency than an equivalent single transistor. As discussed earlier, the price to pay for these superior characteristics would be the slower switching speed and the added complexity. Overall, the Darlington system is ideal when the control signal T_N varies only in the low-temperature regime.

2. *Optical field-based control mechanism*

Similarly to the previous section, the characteristic curves for steady-state energy flows, amplification factors and sensitivity of the optically controlled Darlington pair is presented in Figs. 6 and 7. The optical Rabi frequency Ω_F now replaces T_N as the control parameter, and the optical energy flow rate J_F from the external driving field to the system is added to the curves. The two factors introduced in Eq. (38) also need to be slightly modified to fit the new control parameter as

$$\beta_{\rm Op} = \frac{J_H}{J_F}, \quad \eta^P_{\rm Op} = \frac{\partial J_P}{\partial \Omega_F}. \tag{39}$$

Additionally, the comparison is performed against a single optically controlled thermal gate modelled with the parameters given by Eq. (35).

According to Fig. 6 the Darlington pair still operates as an optically controlled gate, by regulating the majority heat flows J_H and J_C in accordance with Ω_F while consuming very little energy from the optical field. Moreover, it achieves this flow regulation at much lower optical field strengths than the individual device. Consequently, it also reaches saturation faster, as evidenced by the $\eta^P_{\rm Op}$ characteristics in Fig. 7. The thermal efficiency figures are considerably higher too, at least up until saturation sets in.

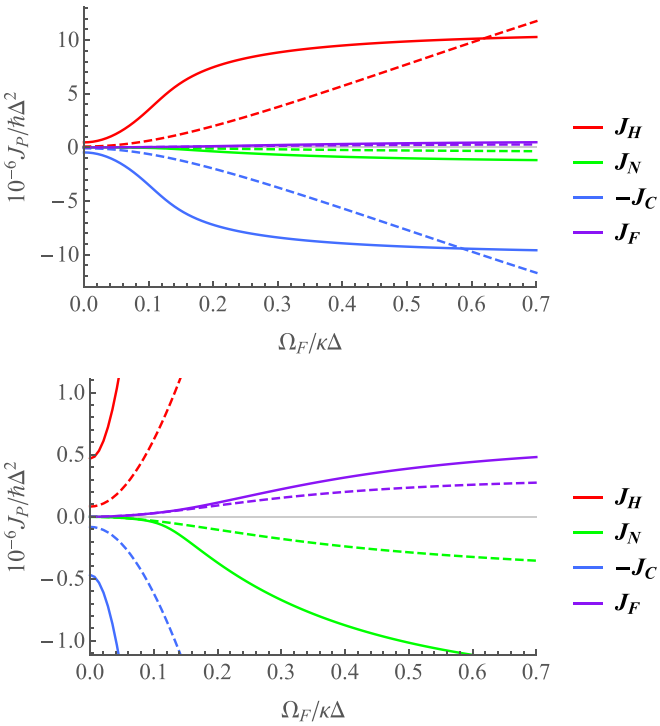

FIG. 6. (Solid) Overall steady-state energy flow rates for the external optical field F and the thermal baths B_H, B_N, and B_C of the optically controlled configuration of the Darlington pair system for $\Omega_F = [0, 0.7\kappa\Delta]$ range. (Dashed) For comparison, the same figures if the Darlington pair is replaced with a single optically controlled thermal gate [25]. All simulation parameters are as given in Sec. III A.

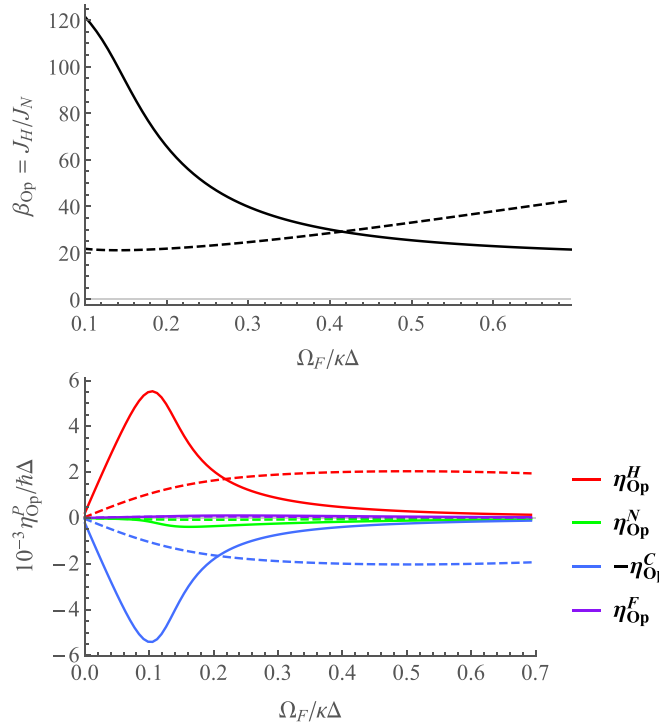

FIG. 7. (Solid) Thermal flow amplification factor $\beta_{\rm Op}$ and thermal flow sensitivity factor $\eta^P_{\rm Op}$ for the optically controlled configuration of the Darlington pair system for $\Omega_F = [0, 0.7\kappa\Delta]$ range. (Dashed) For comparison, the same figures if the Darlington pair is replaced with a single optically controlled thermal gate [25]. All simulation parameters are as given in Sec. III A.

However, unlike in the previous temperature-controlled case, the optically controlled Darlington system is not superior to its single device counterpart across all figures of merit. Specifically, in Fig. 6, we can see how the single device begins to outperform the Darlington pair in terms of the regulated thermal flows in the high Ω_F regime. In fact, when the single device finally reaches saturation at around $\Omega = 3\kappa\Delta$, the values for J_H and J_C is almost four times that of the corresponding saturation values for the Darlington pair. The reason for this behavior is that the optically controlled devices naturally have superior maximum flow capabilities than the temperature-controlled devices, as discovered earlier in [25]. In the Darlington pair, the regulated heat flow always has to go through the transistor S_2. Since S_2 is still controlled by a temperature, the whole system will have inferior maximum heat flows.

The critical advantage of the Darlington pair over an individual transistor for the optically controlled case is that the required operational Rabi frequency range has decreased considerably from $[0, 3\kappa\Delta]$ to around $[0, 0.3\kappa\Delta]$. Furthermore, the thermal flow rates, efficiency and sensitivity are superior within this reduced Ω_F range. The obvious disadvantage, in addition to those discussed previously, is the inferior maximum thermal flows.

Incidentally, these trade-offs for both control mechanisms exactly match those observed in corresponding electronic configurations. Perhaps the most important result of this discussion is the evidence it gives that results from electronic multitransistor systems may be directly carried over to their thermal counterparts under the intermediate bath formalism.

D. Transient characteristics

Before concluding this section, we want to briefly investigate how the Darlington pair responds to a sudden change in the input parameter. We specifically want to see how the relaxation time compares to the single transistor device and how the properties of the intermediate bath affects it. To keep our discussion short, we will only analyze the optically controlled configuration. For simplicity, we have also assumed that the heat capacity C_I of the intermediate bath is a constant independent of the temperature T_I.

In Fig. 8, we present a time-domain analysis of when our systems experience a sudden change in the input optical field. These time domain behaviors were obtained by numerically solving the Eqs. (16), (18), (21), and (27). Initially both systems are stable at their respective steady state for $\Omega_F = 0$. Once the optical field is suddenly increased to $\Omega_F = 0.5\kappa\Delta$, both systems fluctuate for a while before eventually converging to a new steady state.

Naturally, the single transistor must converge faster than the Darlington pair. The time it takes to converge to its steady state can be used to approximate the individual transistor relaxation timescale τ_R we previously introduced in Sec. II B 1. On the other hand, the time the Darlington pair

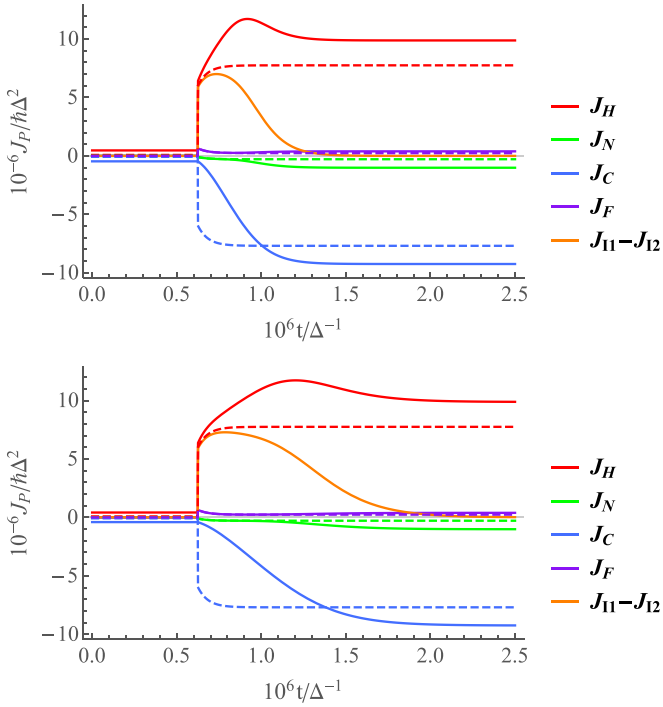

FIG. 8. Transient characteristics of the optically controlled Darlington pair (solid) and its corresponding single transistor (dashed) when optical Rabi frequency is suddenly increased from $\Omega_F = 0$ to $\Omega_F = 0.5\kappa\Delta$. (Top) $C_I = 20k_B$. (Bottom) $C_I = 40k_B$. All other simulation parameters are as given in Sec. III A.

takes to relax depends upon the heat capacity C_I of B_I. We can clearly see from Fig. 8 that higher heat capacities mean that the system takes longer to reach its steady state. Incidentally, this relaxation time can be used to approximate τ_T in Eq. (28), since T_I fluctuates in the same timescales as $J_{I1} - J_{I2}$.

As mentioned previously, the validity of our time-domain analysis critically depends upon the condition $\tau_T \gg \tau_R$. It is therefore obvious that reducing C_I to the point that both systems have similar convergence rates would make the model itself invalid. From this result, we can infer that the Darlington pair necessarily has to be slower than a single transistor. That aside, we also established earlier that steady-state solutions are valid regardless of the value of C_I. These seemingly contradictory conclusions can be resolved by observing that it is only the transient behaviors that are made invalid when τ_T approaches τ_R. Simply put, the devices will eventually approach the same steady state, but through a different pathway than predicted by our intermediate bath formalism.

IV. FUNCTIONALITY OF THE INTERMEDIATE BATH

In this section, we briefly discuss the role of the intermediate bath B_I in facilitating the thermal energy exchange between the two transistors. We believe an intuitive understanding of these underlying mechanisms will be helpful to inspire further research into other quantum systems that can serve as intermediaries between quantum thermal devices. For our discussion, we will choose the temperature-controlled configuration of the Darlington pair, mainly because both transistors being identical makes the analysis simpler.

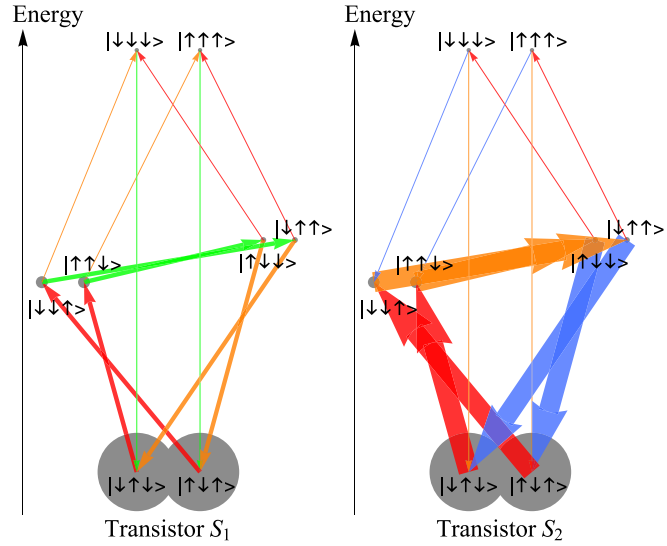

FIG. 9. The state and transition rate diagrams [25] of the two individual thermal transistors in the steady state of the temperature-controlled Darlington pair. The control bath temperature is set at $T_N = 0.4T_H$, corresponding to a partially conducting state of the Dalington pair. The intermediate bath temperature at the steady state is found to be $T_I \approx 0.7T_H$. All other simulation parameters are as given in Sec. III A.

We employ the state and transition diagrams introduced in Ref. [25] to visualize the steady-state operation of each transistor. In Fig. 9, we show these diagrams for a typical steady-state operating condition where the control temperature T_N is large enough to allow a moderate thermal flow through the Darlington pair.

The eight nodes in each diagram of Fig. 9 represent the eight energy levels of the corresponding thermal transistor. The relative size of the grey circles on each node represents the steady-state population ρ^S_{jj} of that energy level. The nodes are arranged in the vertical axis according to their energy, while the horizontal axis is there simply for clarity. Note how the parameter choices in Eq. (34) creates a twofold degeneracy in the eight energy states. While this is not crucial for the transistor operation, it simplifies our discussion since now there is effectively only four energy levels for each transistor.

The colored arrows between the different nodes represent the transition rates $\Gamma^{S,Q}_{jk}$ in Eqs. (18) and (19). The color of each arrow indicates which thermal bath Q the particular transition is induced by, its direction points to the direction of the population flow, and its thickness represents the magnitude of the transition rate. Within this graphical formalism, the transition rates $\Gamma^{S,Q}_{jk}$ are interpreted as "flows" of populations between the nodes while the node sizes are interpreted as the "volume" of populations in each energy eigenstate. Consequently, the steady-state condition can be verified by noting how the arrow thicknesses coming in and going out of each energy node are equal, which ensures that its population remains unchanged.

Any arrow pointing upwards in the energy axis entails an absorption of energy from the corresponding thermal bath, since the transistor moves from a low-energy state to a high-energy state. Conversely, a downward pointing arrow is

associated with an energy release to the respective thermal bath. According to Eq. (24), the total energy flow rate J_Q^S of any thermal bath Q is calculated by taking the product of each transition rate $\Gamma_{jk}^{S,Q}$ with its corresponding energy level difference ϵ_{jk}^S, and summing it over all transitions associated with that bath. Therefore we can easily estimate any J_Q^S from these diagrams by considering the vertical lengths, directions and thicknesses of all the arrows with the appropriate color.

Interestingly, these diagrams offer an intuitive explanation of almost every aspect of the quantum thermal transistor mechanism. We refer the reader to Wijesekara *et al.* [25] for a more detailed discussion. Here, we are concentrating only on the role of the intermediate bath B_I.

From the orange arrows of Fig. 9, we can clearly see that B_I drives the transitions

$$\begin{aligned}
\mathcal{T}_1^{S_1} &= |{\downarrow\downarrow\uparrow}^{S_1}\rangle \rightarrow |{\downarrow\downarrow\downarrow}^{S_1}\rangle,\\
\mathcal{T}_1^{S_1} &= |{\uparrow\uparrow\downarrow}^{S_1}\rangle \rightarrow |{\uparrow\uparrow\uparrow}^{S_1}\rangle,\\
\mathcal{T}_2^{S_1} &= |{\downarrow\uparrow\uparrow}^{S_1}\rangle \rightarrow |{\downarrow\uparrow\downarrow}^{S_1}\rangle,\\
\mathcal{T}_2^{S_1} &= |{\uparrow\downarrow\downarrow}^{S_1}\rangle \rightarrow |{\uparrow\downarrow\uparrow}^{S_1}\rangle
\end{aligned} \tag{40}$$

in S_1, and the transitions

$$\begin{aligned}
\mathcal{T}_1^{S_2} &= |{\downarrow\downarrow\downarrow}^{S_2}\rangle \rightarrow |{\downarrow\uparrow\downarrow}^{S_2}\rangle,\\
\mathcal{T}_1^{S_2} &= |{\uparrow\uparrow\uparrow}^{S_2}\rangle \rightarrow |{\uparrow\downarrow\uparrow}^{S_2}\rangle,\\
\mathcal{T}_2^{S_2} &= |{\downarrow\downarrow\uparrow}^{S_2}\rangle \rightarrow |{\downarrow\uparrow\uparrow}^{S_2}\rangle,\\
\mathcal{T}_2^{S_2} &= |{\uparrow\uparrow\downarrow}^{S_2}\rangle \rightarrow |{\uparrow\downarrow\downarrow}^{S_2}\rangle
\end{aligned} \tag{41}$$

in S_2. Note that we have used the same symbol $\mathcal{T}_i^S$ to denote transitions which are effectively equivalent due to the previously mentioned energy level degeneracy.

We can safely ignore $\mathcal{T}_1^{S_1}$ and $\mathcal{T}_1^{S_2}$ since these transition rates (i.e., thicknesses of the arrows) are much smaller than both $\mathcal{T}_2^{S_1}$ and $\mathcal{T}_2^{S_2}$. We now see that the functionality of the thermal bath B_I is twofold. First, it encourages the downward $\mathcal{T}_2^{S_1}$ transition by absorbing excess thermal energy from the first transistor S_1. Second, it encourages the upwards $\mathcal{T}_2^{S_2}$ transition by providing the required energy to S_2. The steady state is achieved when B_I absorbs as much energy from S_1 as it releases to S_2. The precise temperature T_I that achieves this balance is therefore the steady-state temperature of B_I.

An insightful reader might observe that the $\mathcal{T}_2^{S_1}$ transition has a much larger energy gap than the $\mathcal{T}_2^{S_2}$ transition. For the specific system parameters in Fig. 9, these gaps amount to $1.1\hbar\Delta$ and $0.2\hbar\Delta$ for $\mathcal{T}_2^{S_1}$ and $\mathcal{T}_2^{S_2}$ respectively. This effectively means that the energy released by S_1 in a single downward quantum jump of the $\mathcal{T}_2^{S_1}$ transition is much larger than the energy S_2 can absorb in a single upward jump of the $\mathcal{T}_2^{S_2}$ transition.

This brings to light the most important function of the intermediate bath. It absorbs a relatively large amount of energy from S_1 in a single quantum jump of the $\mathcal{T}_2^{S_1}$ transition, and then proportions that energy out in small pieces to S_2 over the course of multiple quantum jumps of the $\mathcal{T}_2^{S_2}$ transition. In essence, it functions as an energy divider in the quantum scale.

We are now in a position to expand upon our earlier claim that a direct coupling between S_1 and S_2 will not facilitate an efficient thermal transport. Any direct coupling between S_1 and S_2 must still contend with the large energy difference between the donor transition $\mathcal{T}_2^{S_1}$ and recipient transition $\mathcal{T}_2^{S_2}$. To use a different terminology, the coupling between S_1 and S_2 will have to transfer energy under a significantly off-resonant condition. Typically, the coupling strengths will have to be increased at least to ultrastrong levels to overcome the off-resonance issue. However, by that point the energy levels of the two quantum systems will be so severely affected that they can no longer be expected to function as two individual thermal transistors.

This is exactly why we need a third quantum system in the middle to handle the above mentioned proportioning of energy and bypass the off-resonance problem. Our intermediate bath has two important properties which allows it to act efficiently as the intermediary. First, it is made up of a large number of quantum harmonic oscillators, so that both $\mathcal{T}_2^{S_1}$ and $\mathcal{T}_2^{S_2}$ transitions will have to be resonant with at least some of them. Second, any energy that is absorbed into the bath is quickly distributed (i.e., thermalized) among its oscillators. The first property streamlines the energy exchange between the two transistors and the bath, while the second supports efficient thermal energy transport within the bath.

Before concluding this section, we note that there may be other quantum systems beside a thermal bath which can handle this type of energy transport. For instance, a properly tuned quantum harmonic oscillator or a multilevel system may be capable of jumping up multiple energy levels while absorbing a large energy from S_1, and release that energy in parts to S_2 over the course of several relaxation steps. We believe the intuitive mechanisms we described here will assist future researchers in identifying and engineering such systems.

V. CONCLUSIONS

This paper investigated two quantum thermal transistors arranged in a Darlington pair configuration in terms of its thermal behaviors. We investigated two possible control schemes for the Darlington pair. In the temperature-controlled configuration, we used the temperature T_N of an external thermal bath B_N as the control signal. Alternatively, in the optically controlled configuration, the Rabi frequency Ω_F of an external optical field F was used. We employed the previously developed temperature-controlled thermal transistor [17] and optically controlled thermal transistor [25] models to simulate the individual transistors. The whole configuration's expected functionality was to control the thermal energy flow rate between the external thermal baths B_H and B_C by the input signal.

Unlike quantum devices investigated in previous work, the Darlington pair contained two individual transistors exchanging thermal energy through an internal interconnection. It was quite difficult to directly couple the two transistors using a simple interaction Hamiltonian in a manner that facilitated a strong thermal energy transfer. This was because the energy levels of the two transistors which mediate this transfer were significantly off-resonant to each other. Hence, to facilitate the necessary thermal flow through this intermediate junction, we introduced another thermal bath B_I in between the two transistors. After developing a model to characterize the thermal

flow through this intermediary bath, we numerically simulated both the Darlington pair's steady-state and transient thermal flow behaviors.

Our detailed analysis revealed that if the external temperatures and optical fields are held constant, the Darlington pair always relaxed to a single steady state regardless of the initial condition. Analyzing this steady-state behavior, we found that both the temperature-controlled and optically controlled configurations delivered the expected functionality of regulating the thermal flows between B_H and B_C.

For the temperature-controlled configuration, the Darlington pair regulated larger thermal flows at lower input temperatures than an equivalent single thermal transistor. Further analysis showed that the thermal Darlington pair had significantly larger thermal flow amplification, better temperature sensitivity, and superior thermodynamic efficiency. Alternatively, for the optically controlled configuration, the thermal Darlington pair managed to regulate the output thermal flows while requiring only a fraction of the optical field strength demanded by an equivalent single optical thermal transistor. Similarly, the sensitivity and thermodynamic efficiency of the thermal Darlington pair were superior in this reduced input range. However, the Darlington pair saturated at lower thermal flow levels than a single thermal transistor, leading to reduced maximum regulated thermal flows and efficiency in the high Ω_F regime.

These results closely resemble the functionality expected of a Darlington pair in electronics literature. In summary, a thermal Darlington pair modeled after an electronic Darlington pair showed similar characteristics to the electronic case under our intermediate bath formalism. By generalizing this result, future researchers may directly translate electronic multitransistor configurations to their thermal counterparts using this intermediate bath formalism.

A general weakness of using intermediate baths between transistors was the considerable slowing of the composite device's operational speed. The root cause for this was identified as the adiabatic approximation required when incorporating changing temperatures into the individual transistors' models. A potential workaround would be to use a smaller quantum system than a thermal bath as the intermediary between the two devices. A single quantum harmonic oscillator or a multilevel system looks promising in properly mediating the energy flow. Investigation into such scenarios is left as a potential future extension of this work.

ACKNOWLEDGMENTS

R.T.W. would like to thank H. Hapuarachichi and all members of AχL at Monash University including A. Devi, T. Perera and S. Pathiranage for encouragement and insightful discussions.

APPENDIX: DERIVING THE ENERGY-TEMPERATURE RELATION OF THE INTERMEDIATE BATH B_I

Following the well known Caldeira-Legett model [35], the intermediate thermal bath B_I is modelled as an ensemble of quantum harmonic oscillators. According to Eq. (4), its Hamiltonian $\hat{H}^I_{\text{bath}}$ reads

$$\hat{H}^I_{\text{bath}} = \sum_k \hbar\omega^I_k \, \hat{a}^{I\,\dagger}_k \hat{a}^I_k, \tag{A1}$$

where $\hat{a}^I_k$ is the annihilation operator of the k^{th} harmonic oscillator with fundamental frequency ω^I_k. Since the bath is assumed to be under a thermal distribution, its density matrix $\hat{\rho}_I$ is given by

$$\hat{\rho}_I = \frac{\exp\left(-\frac{\hat{H}^I_{\text{bath}}}{k_{\text{B}}T_I}\right)}{\text{Tr}\left\{\exp\left(-\frac{\hat{H}^I_{\text{bath}}}{k_{\text{B}}T_I}\right)\right\}}, \tag{A2}$$

where k_{B} is the Boltzmann constant and T_I is the temperature of B_I.

The average internal energy E^I_{int} of the thermal bath is the expected value of its Hamiltonian [34]. We can calculate this expected value using the elementary relation given in Eq. (22), resulting in

$$E^I_{\text{int}} = \langle \hat{H}^I_{\text{bath}} \rangle = \frac{\text{Tr}\left\{\hat{H}^I_{\text{bath}} \exp\left(-\frac{\hat{H}^I_{\text{bath}}}{k_{\text{B}}T_I}\right)\right\}}{\text{Tr}\left\{\exp\left(-\frac{\hat{H}^I_{\text{bath}}}{k_{\text{B}}T_I}\right)\right\}}. \tag{A3}$$

Working in the number basis with respect to each harmonic oscillator, the trace of any operator $\hat{I}$ reads

$$\text{Tr}\{\hat{I}\} = \sum_{N_1=0}^{\infty} \cdots \sum_{N_k=0}^{\infty} \ldots \langle N_1 \ldots N_k \ldots | \hat{I} | N_1 \ldots N_k \ldots \rangle,$$

where N_k denotes the occupation number of the k^{th} oscillator.

Calculating the two traces in Eq. (A3) and simplifying gives us the relationship between the temperature and the average internal energy of the thermal bath as

$$E^I_{\text{int}} = \sum_k \frac{\hbar\omega^I_k}{\exp\left(\frac{\hbar\omega^I_k}{k_{\text{B}}T_I}\right) - 1}. \tag{A4}$$

Substituting for E^I_{int} in Eq. (25) and carrying out the differentiation results in the relation

$$C_I(T_I) = k_{\text{B}} \sum_k \left(\frac{\hbar\omega^I_k}{k_{\text{B}}T_I}\right)^2 \frac{\exp\left(\frac{\hbar\omega^I_k}{k_{\text{B}}T_I}\right)}{\left[\exp\left(\frac{\hbar\omega^I_k}{k_{\text{B}}T_I}\right) - 1\right]^2}. \tag{A5}$$

We cannot simplify this equation further without fully specifying the frequency distribution (i.e., distribution of the ω^I_ks) of the harmonic oscillator ensemble. However, we can still get some important results for several limiting cases.

First of all, we can easily see that $C_I(T_I) > 0$ for any oscillator distribution. Furthermore, letting ω^I_k go towards zero for all k gives us

$$\lim_{\omega^I_k \to 0} C_I(T_I) = k_{\text{B}} k_{\max}, \tag{A6}$$

where $k_{\max}$ is the number of oscillators in the thermal bath. This means that if the ensemble mostly contains low-frequency oscillators (i.e., $\hbar\omega^I_k \ll k_{\text{B}}T_I$), the heat capacity will be approximately independent of temperature. In that case, the internal energy will have a linear relationship to the temperature, and $E^I_{\text{int}} \propto T_I$.

[1] B. Wang, J. Wang, and H. Guo, Quantum spin field effect transistor, Phys. Rev. B **67**, 092408 (2003).

[2] M. H. Devoret and R. J. Schoelkopf, Amplifying quantum signals with the single-electron transistor, Nature (London) **406**, 1039 (2000).

[3] V. Amendola, R. Pilot, M. Frasconi, O. M. Maragò, and M. A. Iatì, Surface plasmon resonance in gold nanoparticles: A review, J. Phys.: Condens. Matter **29**, 203002 (2017).

[4] T. Perera, S. D. Gunapala, M. I. Stockman, and M. Premaratne, Plasmonic properties of metallic nanoshells in the quantum limit: From single particle excitations to plasmons, J. Phys. Chem. C **124**, 27694 (2020).

[5] W. Zhu, I. D. Rukhlenko, and M. Premaratne, Linear transformation optics for plasmonics, JOSA B **29**, 2659 (2012).

[6] M. Premaratne and M. I. Stockman, Theory and technology of spasers, Adv. Opt. Photonics **9**, 79 (2017).

[7] B. Liu, W. Zhu, S. D. Gunapala, M. I. Stockman, and M. Premaratne, Open resonator electric spaser, ACS nano **11**, 12573 (2017).

[8] C. Jayasekara, M. Premaratne, S. D. Gunapala, and M. I. Stockman, Mos2 spaser, J. Appl. Phys. **119**, 133101 (2016).

[9] H. Wang, Y.-M. He, T.-H. Chung, H. Hu, Y. Yu, S. Chen, X. Ding, M.-C. Chen, J. Qin, X. Yang *et al.*, Towards optimal single-photon sources from polarized microcavities, Nat. Photonics **13**, 770 (2019).

[10] A. Devi, S. D. Gunapala, M. I. Stockman, and M. Premaratne, Nonequilibrium cavity QED model accounting for dipole-dipole interaction in strong, ultrastrong, and deep-strong-coupling regimes, Phys. Rev. A **102**, 013701 (2020).

[11] P. Senellart, G. Solomon, and A. White, High-performance semiconductor quantum-dot single-photon sources, Nat. Nanotechnol. **12**, 1026 (2017).

[12] H. Hapuarachchi, S. D. Gunapala, and M. Premaratne, Plasmonic metaresonances: Harnessing nonlocal effects for prospective biomedical applications, J. Phys.: Condens. Matter **31**, 325301 (2019).

[13] M. Premaratne and G. P. Agrawal, *Light Propagation in Gain Media: Optical Amplifiers* (Cambridge University Press, 2011).

[14] M. Schmotz, J. Maier, E. Scheer, and P. Leiderer, A thermal diode using phonon rectification, New J. Phys. **13**, 113027 (2011).

[15] T. Werlang, M.A. Marchiori, M.F. Cornelio, and D. Valente, Optimal rectification in the ultrastrong coupling regime, Phys. Rev. E **89**, 062109 (2014).

[16] B. Karimi, J. Pekola, M. Campisi, and R. Fazio, Coupled qubits as a quantum heat switch, Quantum Sci. Technol. **2**, 044007 (2017).

[17] K. Joulain, J. Drevillon, Y. Ezzahri, and J. Ordonez-Miranda, Quantum thermal transistor, Phys. Rev. Lett. **116**, 200601 (2016).

[18] D. Hatanaka, I. Mahboob, K. Onomitsu, and H. Yamaguchi, A phonon transistor in an electromechanical resonator array, Appl. Phys. Lett. **102**, 213102 (2013).

[19] B.-q. Guo, T. Liu, and C.-s. Yu, Quantum thermal transistor based on qubit-qutrit coupling, Phys. Rev. E **98**, 022118 (2018).

[20] B.-q. Guo, T. Liu, and C.-s. Yu, Multifunctional quantum thermal device utilizing three qubits, Phys. Rev. E **99**, 032112 (2019).

[21] Y. Zhang, X. Zhang, Z. Ye, G. Lin, and J. Chen, Three-terminal quantum-dot thermal management devices, Appl. Phys. Lett. **110**, 153501 (2017).

[22] Y. Zhang, Z. Yang, X. Zhang, B. Lin, G. Lin, and J. Chen, Coulomb-coupled quantum-dot thermal transistors, Europhys. Lett. **122**, 17002 (2018).

[23] A. Mandarino, K. Joulain, M. D. Gómez, and B. Bellomo, Thermal transistor effect in quantum systems, arXiv:1902.01309.

[24] J. Du, W. Shen, S. Su, and J. Chen, Quantum thermal management devices based on strong coupling qubits, Phys. Rev. E **99**, 062123 (2019).

[25] R. T. Wijesekara, S. D. Gunapala, M. I. Stockman, and M. Premaratne, Optically controlled quantum thermal gate, Phys. Rev. B **101**, 245402 (2020).

[26] C. Elouard, G. Thomas, O. Maillet, J. P. Pekola, and A. N. Jordan, A quantum heat switch based on a driven qubit, Phys. Rev. E **102**, 030102 (2020).

[27] S. Nimmrichter, J. Dai, A. Roulet, and V. Scarani, Quantum and classical dynamics of a three-mode absorption refrigerator, Quantum **1**, 37 (2017).

[28] M. T. Mitchison, M. P. Woods, J. Prior, and M. Huber, Coherence-assisted single-shot cooling by quantum absorption refrigerators, New J. Phys. **17**, 115013 (2015).

[29] M. Majland, K. S. Christensen, and N. T. Zinner, Quantum thermal transistor in superconducting circuits, Phys. Rev. B **101**, 184510 (2020).

[30] R. Scheibner, M. König, D. Reuter, A. Wieck, C. Gould, H. Buhmann, and L. Molenkamp, Quantum dot as thermal rectifier, New J. Phys. **10**, 083016 (2008).

[31] D. A. Hodges, Darlington's contributions to transistor circuit design, IEEE Trans. Circuits Syst. I **46**, 102 (1999).

[32] A. S. Sedra, D. E. A. S. Sedra, K. C. Smith, and K. C. Smith, *Microelectronic circuits* (New York, Oxford University Press, 1998).

[33] See Supplemental Material at http://link.aps.org/supplemental/10.1103/PhysRevB.104.045405 for complete numerical simulations for a Darlington pair of quantum thermal transistors.

[34] H.-P. Breuer, F. Petruccione *et al.*, *The Theory of Open Quantum Systems* (Oxford University Press on Demand, Oxford, 2002).

[35] A. Caldeira and A. J. Leggett, Quantum tunnelling in a dissipative system, Ann. Phys. **149**, 374 (1983).

[36] M. Premaratne and G. P. Agrawal, *Theoretical Foundations of Nanoscale Quantum Devices* (Cambridge University Press, London, 2021).

[37] C. A. Brasil, F. F. Fanchini, and R. d. J. Napolitano, A simple derivation of the lindblad equation, Revista Brasileira de Ensino de Física **35**, 01 (2013).

[38] A. J. Leggett, S. Chakravarty, A. T. Dorsey, M. P. Fisher, A. Garg, and W. Zwerger, Dynamics of the dissipative two-state system, Rev. Mod. Phys. **59**, 1 (1987).

[39] N. De Silva, T. K. Warnakula, S. D. Gunapala, M. I. Stockman, and M. Premaratne, Effect of logarithmic perturbations in ohmic like spectral densities in dynamics of electronic excitation using variational polaron transformation approach, J. Phys.: Condens. Matter **33**, 145304 (2021).

[40] A. Rivas, A. D. K. Plato, S. F. Huelga, and M. B. Plenio, Markovian master equations: A critical study, New J. Phys. **12**, 113032 (2010).

[41] P. P. Hofer, M. Perarnau-Llobet, L. D. M. Miranda, G. Haack, R. Silva, J. B. Brask, and N. Brunner, Markovian master equations for quantum thermal machines: Local versus global approach, New J. Phys. **19**, 123037 (2017).

[42] C. Elouard, D. Herrera-Martí, M. Esposito, and A. Auffèves, Thermodynamics of optical bloch equations, New J. Phys. **22**, 103039 (2020).

[43] D. Halliday, R. Resnick, and J. Walker, *Fundamentals of Physics* (John Wiley & Sons, New York, 2013).

[44] A. Blais, A. L. Grimsmo, S. M. Girvin, and A. Wallraff, Circuit quantum electrodynamics, Rev. Mod. Phys. **93**, 025005 (2021).

[45] J. Roßnagel, S. T. Dawkins, K. N. Tolazzi, O. Abah, E. Lutz, F. Schmidt-Kaler, and K. Singer, A single-atom heat engine, Science **352**, 325 (2016).

[46] H. Paik, D.I. Schuster, L. S. Bishop, G. Kirchmair, G. Catelani, A.P. Sears, B.R. Johnson, M.J. Reagor, L. Frunzio, L. I. Glazman, S. M. Girvin, M. H. Devoret, R. J. Schoelkopf, Observation of High Coherence in Josephson Junction Qubits Measured in a Three-Dimensional Circuit Qed Architecture, Phys. Rev. Lett. **107**, 240501 (2011).

[47] P. P. Hofer, M. Perarnau-Llobet, J. B. Brask, R. Silva, M. Huber, and N. Brunner, Autonomous quantum refrigerator in a circuit qed architecture based on a josephson junction, Phys. Rev. B **94**, 235420 (2016).